Real-Time, In Situ Monitoring of the Oxidation of Graphite: Lessons Learned

Naoki Morimoto,[a] *Hideyuki Suzuki,*[b] *Yasuo Takeuchi,*[a] *Shogo Kawaguchi,*[c] *Masahiro Kunisu,*[d] *Christopher W. Bielawski,*[e,f] *and Yuta Nishina*[b,g]*

[a] Graduate School of Medicine, Dentistry, and Pharmaceutical Sciences, Division of Pharmaceutical Sciences, Okayama University, 1-1-1 Tsushimanaka, Kita-ku, Okayama 700-8530, Japan

[b] Research Core for Interdisciplinary Sciences, Okayama University, 3-1-1 Tsushimanaka, Kita-ku, Okayama 700-8530, Japan

[c] Japan Synchrotron Radiation Research Institute (JASRI), SPring-8, Sayo, Hyogo 679-5198, Japan

[d] Toray Research Center, Inc., Surface Science Laboratories, 2-1 Sonoyama 3-chome, Otsu, Shiga, 520-0842, Japan

[e] Center for Multidimensional Carbon Materials (CMCM), Institute for Basic Science (IBS), Ulsan 44919, Republic of Korea

[f] Department of Chemistry and Department of Energy Engineering, Ulsan National Institute of Science and Technology (UNIST), Ulsan 44919, Republic of Korea

[g] Precursory Research for Embryonic Science and Technology, Japan Science and Technology Agency, 4-1-8 Honcho, Kawaguchi, Saitama 332-0012, Japan

<Abstract>

Graphite oxide (GO) and its constituent layers (i.e., graphene oxide) display a broad range of functional groups and, as such, continue to attract significant attention for use in numerous applications. GO is commonly prepared using the "Hummers method" or a variant thereof where graphite is treated with $KMnO_4$ and various additives in H_2SO_4. Despite its omnipresence, the underlying chemistry of such oxidation reactions is not well understood and typically afford results that are irreproducible and, in some cases, unsafe. To overcome these limitations, the oxidation of graphite under Hummers-type conditions was monitored over time using in situ X-ray diffraction (XRD) and in situ X-ray absorption near edge structure (XANES) analyses with synchrotron radiation. In conjunction with other atomic absorption spectroscopy, UV-Vis spectroscopy and elemental analysis measurements, the underlying mechanism of the oxidation reaction was elucidated and the reaction conditions were optimized. Ultimately, methodology for reproducibly preparing GO on large scales using only graphite, H_2SO_4, and $KMnO_4$ was developed and successfully adapted for use in continuous flow systems.

<Introduction>

Although graphite oxide (GO) has been known for more than 150 years, its individual layers, often termed graphene oxide, have recently gained extraordinary attention for potential use in a broad range of applications.[1–8] The attraction is due, in part, to the material's high chemical potential, which stems from the myriad functional groups decorated on its surface. GO is typically prepared by treating graphite with a strong oxidizer followed by exfoliation, and many variations

of this methodology exist.[9–12] An early (1958) yet recently popular (>10,000 citations over the past five years) method was reported[13] by Hummers *et. al.* who demonstrated that GO may be obtained by exposing graphite to a mixture of $KMnO_4$ and $NaNO_3$ in H_2SO_4. Subsequent variations of this method have enabled access to single-layer GO and other forms of oxidized carbons.[14–17] Despite its prevalence, the underlying chemistry of the Hummers' method is not well understood and varying or irreproducible outcomes are often obtained despite many experimental[18, 19] and computational[20–24] studies.

While *in situ* analyses of Hummers-type oxidations could help to enrich our understanding of the underlying mechanism(s), such reactions are typically performed in concentrated H_2SO_4 and in the presence of a strong oxidant which excludes the use of conventional characterization techniques, such X-ray photoelectron spectroscopy (XPS), FTIR spectroscopy, and elemental analysis. To overcome this limitation, we utilized in situ X-ray diffraction (XRD) and in situ X-ray absorption near edge structure (XANES) analyses with synchrotron radiation to monitor the oxidation of graphite under the aforementioned conditions. These data in conjunction with a series of atomic absorption spectroscopy, UV-Vis spectroscopy and elemental analysis measurements enabled the Hummers-type oxidation of graphite to be optimized. Ultimately, we found that additives, such as $NaNO_3$, were not necessary to form GO. A simple recipe that consists of only graphite, H_2SO_4, and $KMnO_4$ facilitated the efficient oxidation of graphite.

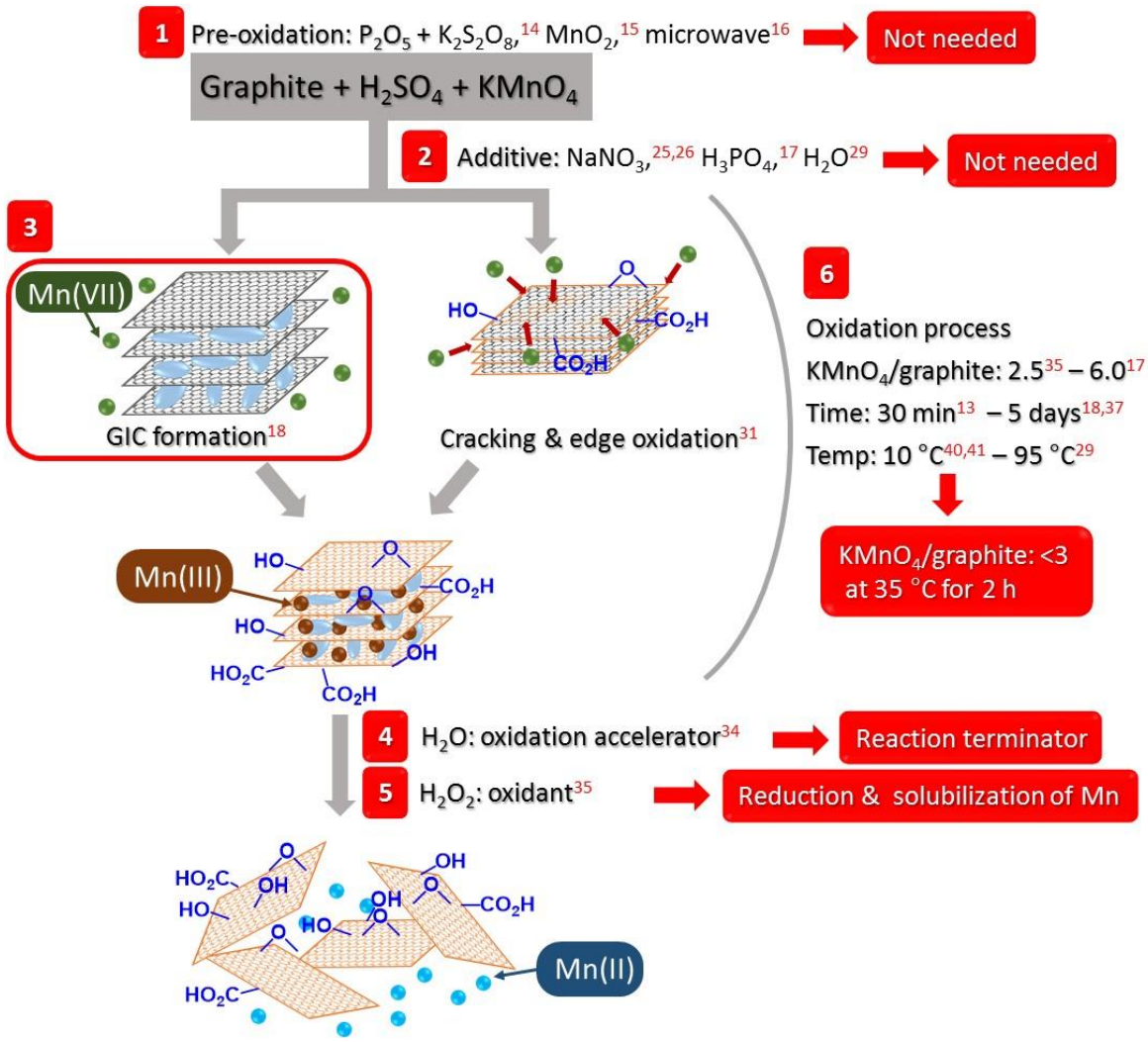

Figure 1. Summary of various Hummers' methods used to oxidize graphite to GO and conclusions drawn from the experiments described herein (red boxes). The numbers in the red boxes refer to the various steps of the reaction and are shown in order.

<Results and Discussion>

Synthesis of GO: The Essentials

According to the original Hummers' procedure, graphite should be suspended in H_2SO_4 and treated with 50 wt.% of $NaNO_3$ followed by the addition of 300 wt.% of $KMnO_4$.[13] Over the course of the reaction, $NaNO_3$ converts to various noxious and environmentally-unfriendly gases; thus,

analogous methods that do not utilize this salt are desired. For example, Kovtyukhova demonstrated that graphite may be pre-treated with P_2O_5 and $K_2S_2O_8$ in H_2SO_4 in lieu of $NaNO_3$.[14] Likewise, Tour reported a method that utilizes H_3PO_4 instead of $NaNO_3$.[17] Alternatively, pre-treating graphite with MnO_2[15] or exposure to microwave radiation[16] has also been shown to promote the formation of GO (Figure 1, step 1 and 2). The Tour group reported that the initial step in Hummers-type oxidation methodologies is the formation of a graphite intercalated compound (GIC).[18] Since it is known that GICs can form in the presence of an oxidant, the $NaNO_3$ and other additives may facilitate graphite interlayer expansion and promote the insertion of the manganese-based reagent,[25, 26] although $KMnO_4$ has also been shown to form GICs as well.[27, 28] The chemical reactions between graphite and $NaNO_3$ or $KMnO_4$ were independently monitored by XRD, and it was determined that GICs were formed in both cases. As shown in Figure S1, as little as 1 wt.% of $KMnO_4$ with respect to graphite was needed to successfully form a GIC. It was also observed that graphite underwent oxidation in the absence of $NaNO_3$, although the intensity of the signals assigned to the presence of C–O bonds, as determined by XPS, was slightly lower when compared to reactions that included $NaNO_3$. Regardless, the product obtained using only $KMnO_4$ was subsequently exfoliated to single-layer GO via sonication and the elemental composition was measured to be similar to an analogous material prepared using $KMnO_4$ and $NaNO_3$. Based on these results, the role of $NaNO_3$ did not appear to be significant and subsequent experiments were performed without this reagent.

Shi previously noted that water enhances the oxidation of graphite (Figure 1, step 2).[29] Building on this observation, a series of GO samples were synthesized in the presence of various quantities of water (0.001 – 20 vol.%) and then characterized using XPS as well as elemental composition

analysis. Although XPS showed that a product with a relatively high oxygen content was formed when the reaction medium was comprised of 20 vol.% water (Figure S2a), elemental analysis indicated that the GO contained the lowest quantity of oxygen (Figure S2b). To resolve this discrepancy, the products were characterized using optical microscopy. From these studies, it was determined that complete exfoliation did not occur when 20 vol.% of water was used (Figure S2c). Since water facilitates the removal of intercalated metal species,[30] any excess may have prevented the intercalation of Mn and resulted in surface oxidation exclusively. Shi also proposed that O_3, formed from water and $KMnO_4$, enhances the oxidation of graphite.[29] Under such conditions, the oxygen atoms on GO should be at least partially derived from water. To examine the extent, if any, to which O_3 influences the oxidation reaction, $H_2[^{18}O]$ was added to the reaction mixture and the resultant GO product was subjected to TGA-mass spectrometry (TGA-MS); the isotopically-enriched byproducts $C[^{18}O]$ and $C[^{18}O]_2$ were observed in relatively small quantities (Figure S3). Based on these results, we concluded that the pre-oxidation graphite is not necessary and that the key reagents needed to facilitate Hummers-type oxidations are $KMnO_4$ and concentrated H_2SO_4. In addition, the use of less than 5 vol.% of water was found to facilitate the formation of single-layer GO after sonication.

Time Course Analyses of the Graphite Oxidation Process

The oxidation of graphite has been proposed to proceed via a GIC[18] or through a process that involves unzipping of the graphite surfaces and edges (Figure 1, step 3).[31] The structural changes that graphite undergoes under oxidative conditions were monitored over time using XRD with synchrotron radiation ($\lambda = 0.8$ Å).[32] A signal derived from graphite ($2\theta = 13.9°$) disappeared almost immediately upon the addition of $KMnO_4$, and a new signal assigned to a GIC appeared at a lower

diffraction angle (2θ = 11.8°, Figure 2a (ii)) without a significant loss in the peak intensity, a result consistent with the formation of a well-organized GIC at an initial stage. Afterward, the intensity of the new signal gradually decreased over time (Figure 2a (iii)) and was absent after 60 min (Figure 2a (iv)). In parallel, a new signal, which was assigned to the formation of Mn- and/or H_2SO_4-intercalated GO, appeared at 2θ = 5.8 ° (d = 0.79 nm) (Figure 2b (iii)). Although the intensity of this signal was relatively low when compared to signals derived from pristine graphite or the GICs, it was consistent with analogous data reported in the literature (0.78 nm).[18] The size of graphite was also found to affect the intercalation process: when relatively large graphite particles (average particle size: 150 μm) were used, a mixture of graphite and GIC were observed after 1 min, and the GIC remained intact for more than 90 min (Figure S6b). In contrast, the use of relatively small graphite particles (average particle size: <75 μm) resulted in a single signal that was attributed to the formation of a GIC. Thus, we concluded that the structure of graphite becomes completely disordered within approximately 1 h after exposure to $KMnO_4$ under acidic conditions.

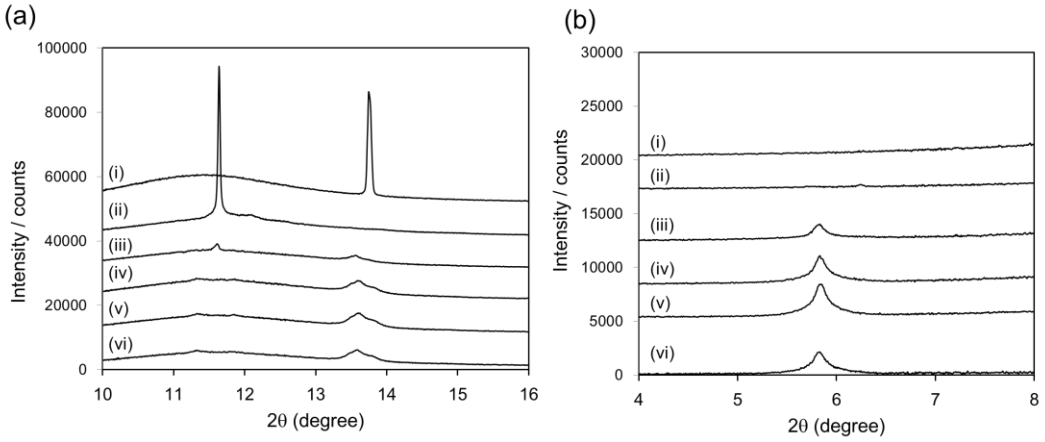

Figure 2. In situ XRD spectra recorded for graphite (i) and after exposure to $KMnO_4$ and H_2SO_4 for (ii) 1 min, (iii) 30 min, (iv) 60 min, (v) 90 min, and (vi) 120 min.

Inspection of the data revealed that there was no clear correlation between the degree of disorder and the extent of graphite oxidation. As graphite is oxidized with $KMnO_4$, the Mn undergoes reduction; therefore, an analysis of the oxidation state of the Mn over the course of the reaction may correlate with the extent of the reaction. The active species involved in the oxidation of graphite is Mn_2O_7 or MnO_3^+,[33] and the oxidation reaction may initiate upon the intercalation of these species into the layers of graphite. To better understand the reaction mechanism, the concentration of Mn in the liquid phase over the course of the oxidation reaction was followed by atomic absorption spectroscopy (Figure 3a). A signal attributed to Mn attenuated by approximately 50% after 10 min of reaction time, and nearly 85% after 120 min. These results were consistent with an accumulation of Mn in the layers of graphite. Next, the consumption of Mn(VII) species and the oxidation degree of graphite was evaluated by UV-Vis spectroscopy. In concentrated H_2SO_4, $KMnO_4$ is converted to Mn_2O_7 or MnO_3^+, which is then transformed to MnO_4^- in the presence of water. Since MnO_4^- is readily reduced in the presence of lower valent Mn species, samples were centrifuged and filtered to remove any undissolved Mn-containing compounds, and then diluted with water. Using this methodology, it was determined that 40% of the Mn(VII) species were consumed within 10 min and were nearly completely consumed within 120 min or upon the addition of water (Figure 3b (▲)). Conversely, the oxygen content of the oxidized graphite gradually increased over time (Figure 3b (○)). The size of graphite also affected the intercalation process as relatively slow consumption rates of the Mn(VII) species were measured when relatively large graphite particles were used (Figure S6).

Since the consumption rate of Mn(VII) and the average oxidation state of the Mn-containing species over the course of the oxidation reaction can serve as benchmarks to estimate the progress of the formation of GO, a series of in situ XANES experiments were performed. Inspection of a series of Mn standards (Figure S4) revealed that a characteristic Mn(VII) pre-edge peak was observed at 6542 eV and that the main absorption regions of each spectra shifted to lower energies as the oxidation state of Mn was reduced. As such, the intensity of the pre-edge signal and the position of the main absorption were used to measure the consumption of Mn(VII) species as well as the average oxidation state of Mn in the reaction mixture over time. As summarized in Figure 3, the intensity of the pre-edge signal derived from the Mn(VII) species gradually decreased over time and was consistent with the consumption rate measured using UV-Vis spectroscopy. Since the XANES spectra did not significantly change after 4 h, we concluded that the oxidation of graphite was complete. A XANES spectrum recorded for the centrifuged reaction mixture before the addition of water was also recorded. While the liquid phase of the mixture showed a relatively strong pre-edge signal that was assigned to Mn(VII) (Figure 3c), the species was not observed in the solid phase (Figure 3d). Collectively, these results suggested to us that Mn(VII) species undergo gradual intercalation but rapid reduction in the graphite layers. Our conclusion that graphite undergoes oxidation within 2-4 h was consistent with that of Kovtyukhova *et al.*, who reported that graphite requires > 30 min to transform to GO under oxidative conditions.[14] At the end of the reaction (120 min), the average oxidation state of the Mn species was determined by the position of main absorption region to be +3. Thus, the stoichiometry of oxygen atoms that were transferred from the $KMnO_4$ to the graphite was calculated to be approximately two (2). Based on the Mn degree of reduction, the utilization efficiency of oxygen atoms from $KMnO_4$ was determined to be 84% (see ESI).

Park[34] and Zhang[35] reported that graphite oxidation reaction progresses upon the addition of water and H_2O_2 (Figure 1, step 4 and 5); however, such outcomes were not observed in the experiments described herein. The difference may be due to the quantities of $KMnO_4$ and water employed. The roles of water and H_2O_2 were clarified by analyzing the change in concentration of the liquid phase of the reaction mixture and oxidation state of the Mn reagent. When water was added, the signal assigned to Mn(VII) completely disappeared and nearly all of the Mn species were contained in the liquid phase (Figure 3). The reason for the disappearance of the signal may be due to comproportionation of Mn(VII) and a reduced Mn (e.g., Mn(III)) species that deintercalated from the GO layers. Collectively, these results indicate that water terminated the oxidation reaction. Using atomic absorption spectroscopy (Figure 3) and SEM-EDS (Figure 4), it was determined that the Mn species may gradually deposit on the GO after the addition of water and that the insoluble Mn species convert to soluble Mn(II) derivatives upon the addition of H_2O_2. Thus, H_2O_2 appears to facilitate the solubilization of the Mn species, which enables the purification of GO by filtration or centrifugation.

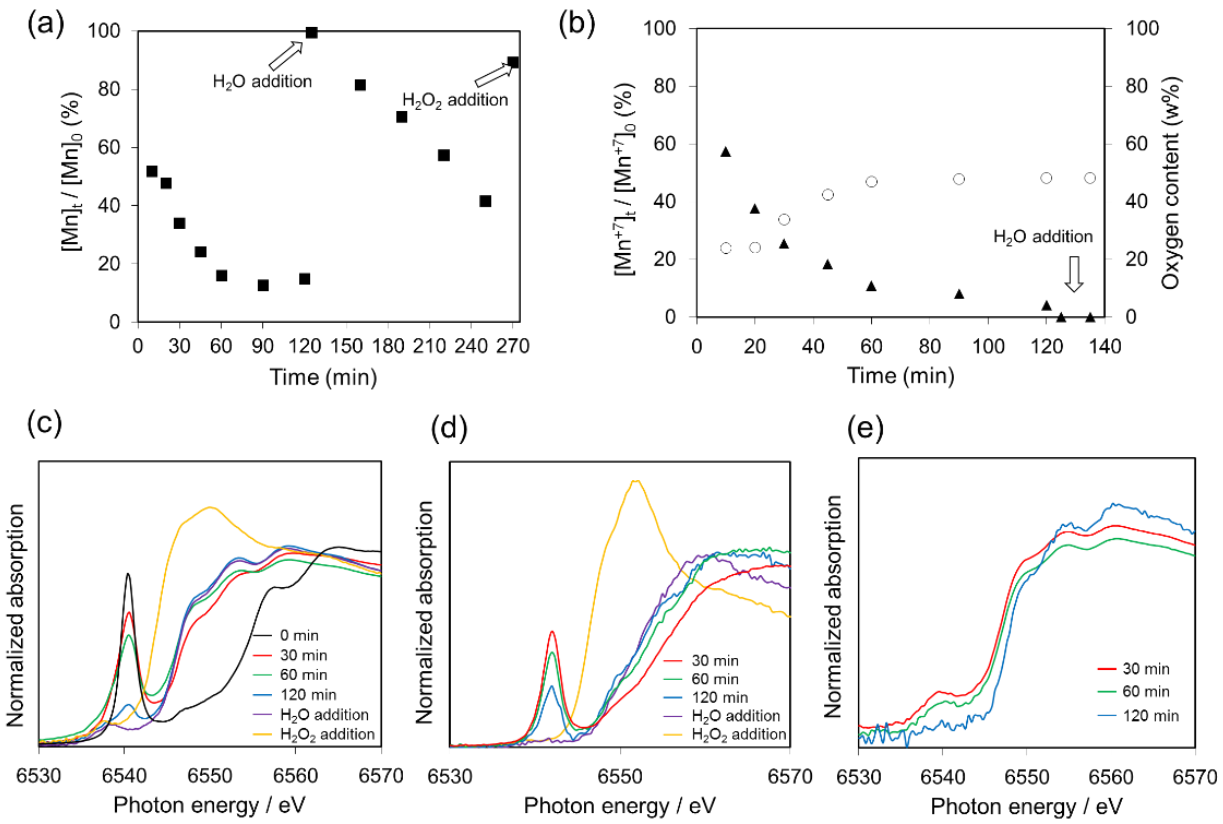

Figure 3. (a) Time-course analysis of the ratio of Mn in the liquid phase (■) of a graphite oxidation reaction as determined using atomic absorption spectroscopy. (b) Time-course analysis of the decrease of Mn(VII) species (▲) as determined via UV-Vis spectroscopy and by monitoring the oxygen content of the respective GO products using CHNS elemental analysis (○). (c) In situ XANES analysis of the oxidation of graphite over time (indicated). (d) Time-course XANES analysis of the supernatant of the reaction mixture. (e) Time-course XANES analysis of the solid product.

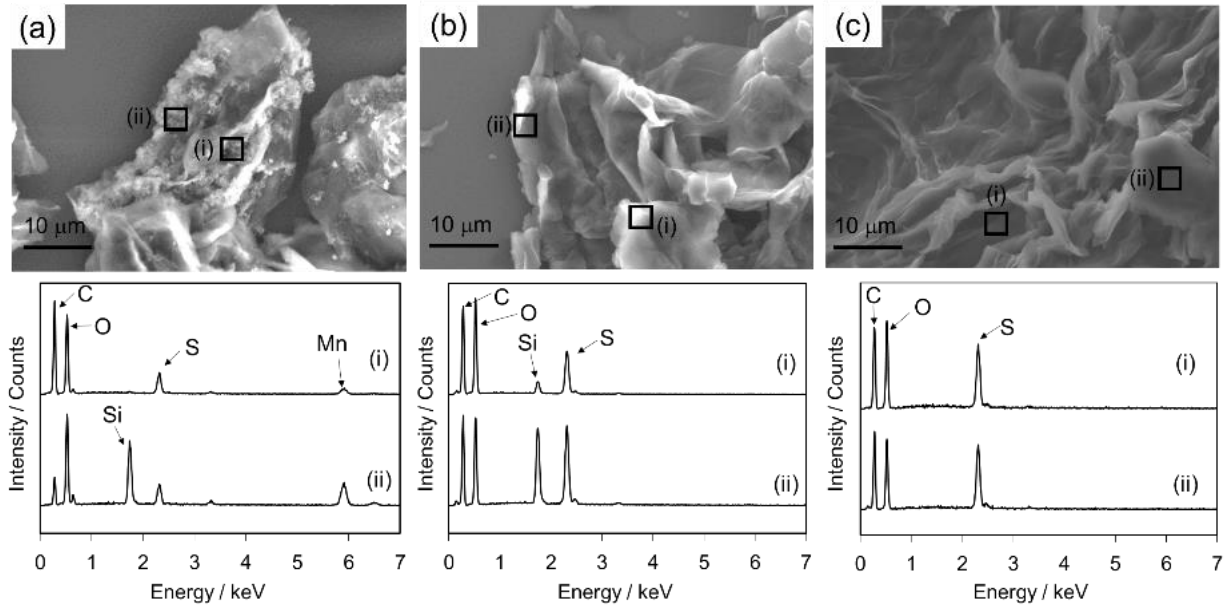

Figure 4. SEM-EDX analyses of GO prepared (a) without H_2O_2, (b) with H_2O_2 and (c) with citric acid in lieu of H_2O_2.

Optimum Oxidation Conditions

In the original Hummers method as well as in modified derivatives, the mass ratio of the $KMnO_4$ and graphite employed is typically within the range of 2.5[36] - 6[17] and reaction is typically performed for periods that range from 30 min[13] to 5 days (Figure 1, step 6).[18, 37] It is well known that excess $KMnO_4$ results in the formation of defects and promotes overoxidation,[38, 39] and longer reaction periods may decompose the product.[31] Nishina reported that the oxygen content of the GO product correlates with the quantity of $KMnO_4$ employed,[36] although the further increase of oxygen content was not observed when the initial ratio of $KMnO_4$ to graphite was >3 (Table S1). The relationship may be due to the elimination of CO_2 which competes with the oxidation of GO in the presence of excess $KMnO_4$. Similarly, we also found that the reaction temperature was an important parameter. In the modified Hummers-type methods, the reaction temperature has been

reported to range from 10 °C[40, 41] to 95 °C[29]. However, when the reaction was performed at relatively high temperatures, defective GO was formed, presumably due to the formation of large quantities of CO_2 (Table 1, Entry 1). In contrast, when analogous reactions were performed at 35 °C, GO was obtained without formation of significant quantities of CO_2 (Table 1, Entry 2). Moreover, reducing the temperature to 10 °C did not result in the formation of CO_2 or the desired product (Table 1, Entry 3, Figure S10). When the reaction was performed for a longer period of time (24 h) and/or the ratio of graphite/$KMnO_4$ was increased, greater quantities of CO_2 were observed (Table 1, Entry 4-6). Based on these observations, it was concluded that the oxidation reaction should be performed near 35 °C for 2 h to obtain high quality GO in high yield (Figure 1, step 6).

Table 1. Evolution of CO_2 under different reaction conditions.[a]

Entry	Graphite (g)	$KMnO_4$ (g)	Time (h)	Temp. (°C)	CO_2 (mg)
1	3	9	2	80	384.6
2	3	9	2	35	6.2
3	3	9	2	10	-
4	3	9	24	35	22.9
5	3	15	2	35	13.6
6	3	15	24	35	101.6
7	0	9	2	35	-

[a] Graphite (3.0 g) was stirred in 95% w/w H_2SO_4 (150 mL) on an ice bath and $KMnO_4$ (amount indicated) was slowly added to the solution to maintain a reaction temperature of <10 °C. The mixture was then stirred at 35 or 80 °C for a period of time (indicated). Liberated CO_2 was trapped using a saturated aqueous solution of $Ba(OH)_2$. The resulting product, $BaCO_3$, was collected by filtration and the weighed to calculate the quantity of CO_2 generated over the course of the oxidation reaction.

Quenching the reaction prior to purification is also required. As such, various reducing agents to convert insoluble Mn(III) to soluble Mn(II) species were screened, including $NaBH_4$, hydrazine and ascorbic acid. Ultimately, it was determined that citric acid was a selective reducing agent for Mn, and can successfully remove the Mn species from GO (Figure 4c, Figure S9).

In the conventional Hummers-type methods, $KMnO_4$ is added at <10 °C, and then the resulting mixture is heated to 35 °C. However, when GO was synthesized on a large scale (500 g), the temperature of the reaction mixture exceeded 50 °C even when a water bath was used as the coolant. Indeed, controlling the temperature of graphite oxidation reactions can be challenging for multiple reasons: 1) Mn_2O_7 formed from $KMnO_4$ and H_2SO_4 has been reported[42] to explode at temperatures exceeding 55 °C, 2) defects are introduced upon elimination of CO_2 at elevated temperatures (e.g., see Table 1), 3) the oxidation reaction is highly exothermic (Figure S8), and 4) the oxidation does not proceed at temperatures below 20 °C (Figure S10). We surmise that large-scale reactions can result in the accumulation of Mn(VII) species which exothermically react with graphite and causes rapid temperature elevation. To overcome these limitations and to develop a safe and efficient synthesis of GO, a continuous flow system was devised (see Figure 5). A solution of $KMnO_4$ in H_2SO_4 was cooled to <10 °C and a separate suspension of graphite in H_2SO_4 was kept at room temperature before mixing. Teflon-coated plunger pumps were adjusted to 1 mL/min and an appropriate volume of tubing (6.25 mm OD, 5.15 mm ID), heated at 35 °C, was used to limit the residence period to 2 h. The product mixture was fed into an aqueous solution of citric acid at <10 °C to quench the reaction. Ultimately, the system facilitated an efficient and continuous production of GO, as determined via SEM and other techniques (Figure 5, Table S3).

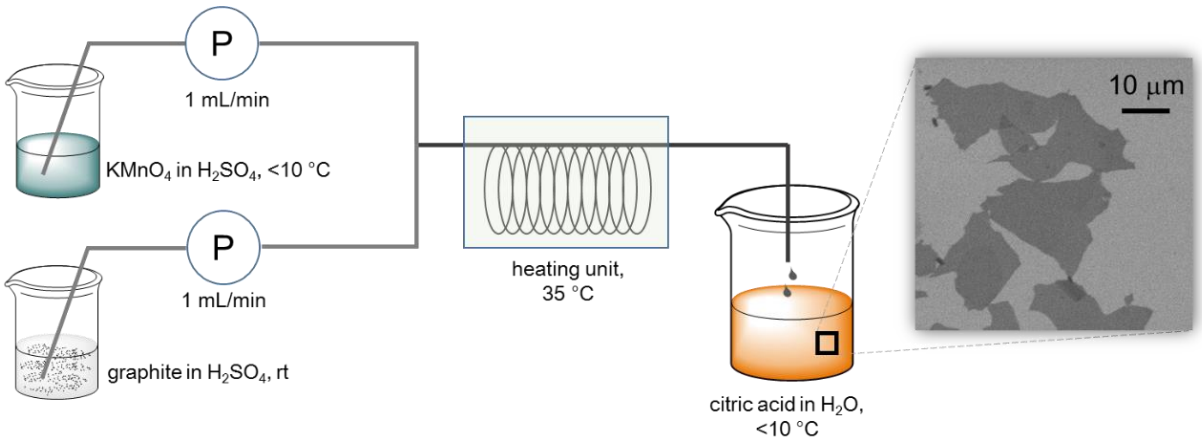

Figure 5. (left) Basic design of a continuous-flow system used to synthesize GO. (right) SEM image of a flake of GO obtained from the continuous-flow system after exfoliation using sonication.

<Conclusion>

We have clarified the essential reagents and reaction conditions required to oxidize graphite to GO in high efficiency and consistency. A series of in situ analyses facilitated the elucidation of the optimal reaction conditions, and revealed the roles of water and H_2O_2: water effectively decomposes Mn(VII) to terminate the oxidation reaction whereas H_2O_2 enhances the solubility of various Mn species. It was also discovered that H_2O_2 could be replaced with a mild reducing agent, such as citric acid, without detriment to the outcome of the reaction. We also demonstrated that GO can be prepared using a continuous-flow system, which enables a relatively safe and reproducible method to prepare the material on large scales.

<Methods>

Optimized Synthesis of GO

Graphite (500 mg) was stirred in 95 wt.% H_2SO_4 (25 mL). $KMnO_4$ (1.5 g) was gradually added to the solution while keeping the temperature <10 °C using an ice bath. The mixture was then stirred at 35 °C for 2 h. The resulting mixture was diluted by water (25 mL) under vigorous stirring and cooling so that the temperature did not exceed 50 °C. The suspension was further treated with 30 wt.% aq. H_2O_2 (1.25 mL). The resulting suspension was purified by repeated centrifugation from water.

Methodology

The in situ XRD analysis were performed at the BL02B2 beamline at SPring-8, Japan. The incident X-ray beam was monochromated to 15.5 keV (λ = 0.8 Å) using a Si (111) double-crystal. The high-resolution diffraction patterns in the Debye-Scherrer transmission geometry were recorded using multiple microstrip solid state detectors (Dectris Ltd. MYTHEN modules). The in situ XAFS measurements were performed at the BL12C beam line at the Photon Factory (PF), KEK (Tsukuba, Japan) using a Si (111) double crystal monochromator and a bent cylindrical mirror that reflected synchrotron radiation from the 2.5 GeV storage ring. The XAFS spectra were measured in a fluorescence-yield mode. The intensities of incident X-ray beams were monitored by a nitrogen-filled ionization chamber, while the fluorescence X-ray signals were detected with a Lytle detector. Other XRD analyses were performed using an PANalytical Co. X' pert PRO with Cu Kα radiation (λ = 1.541 Å) in the 2θ range of 2.0 - 75°. The operating tube current and voltage were 45 mA and 40 kV, respectively. The data were collected at a step size of 0.017° and the scan type was continuous. XPS measurements were performed using a SHIMADZU Kratos AXIS-ULTRA DLD spectrometer with pass energy of 20 eV. CHNS elemental analyses were performed using a PERKINELMER 2400II instrument. Atomic absorption spectroscopy data were recorded

using a SHIMADZU AA-6300 spectrometer and calibrated with 0, 0.1, 0.3, 0.5, 0.75 μM of a standard aqueous manganese solution or 1.0, 2.0, 3.0, 5.0, 7.5, 10.0 μM of a standard aqueous potassium solution. UV-Vis spectroscopy was measured using a JASCO V-670 spectrometer and calibrated with 0, 0.05, 0.1, 0.15, 0.2, 0.3 mM of a standard aqueous $KMnO_4$ solution. SEM and SEM-EDS analyses were performed using a JEOL JSM-IT100 microscope on a SiO_2/Si substrate. Optical microscope images were taken using a LEICA DM2760 microscope on a non-reflecting glass substrate. TGA was performed using a RIGAKU Thermo plus EVO2 analyzer using N_2 as the carrier gas (300 mL/min) and at a heating ramp rate of 6 °C/min. TGA-MS was performed using a SHIMADZU GC-MS QP2010 analyzer using He (99.999%) as a carrier gas (300 mL/min) and at a heating ramp rate of 6 °C/min. The MS measurement was performed in the SIM mode to detect target molecules. The GO was dried using a ADVANTEC DRZ350WC lyophilizer prior to CHNS elemental analysis, XPS, TGA, or TGA-MS. Additional procedures are described in the Supporting Information.

ASSOCIATED CONTENT

Supporting Information. The Supporting Information is available free of charge on the ACS Publications website at DOI:

Formation of GICs, effect of water, exploring graphite size effects, analysis of surface adsorbed water on GO, calculation of the oxidant efficiency, measurement of temperature changes, removal of the residual Mn from GO, degree of oxidation and defect formation.

AUTHOR INFORMATION

Corresponding Author

E-mail: nisina-y@cc.okayama-u.ac.jp

Author Contributions

N.M. and Y.N. performed the graphite oxidation experiments. S.H. and S.K. performed the in situ XRD experiments. M.K. performed in situ XANES experiments. Y.T. and C.W.B. designed the experiments and discussed the data. C.W.B. and Y.N. wrote the manuscript.

Funding Sources

Y.N. is grateful to JST PRESTO and JSPS KAKENHI (Science of Atomic Layers (SATL)) Grant Number 16H00915 for financial support. C.W.B. is grateful to the IBS (IBS-R019-D1) and the BK21 Plus Program funded by the Ministry of Education and the National Research Foundation of Korea for their support.

REFERENCES

1. Dreyer, D. R.; Todd, A. D.; Bielawski, C. W. Harnessing the Chemistry of Graphene Oxide. *Chem. Soc. Rev.* **2014**, *43*, 5288–5301.

2. Zhu, Y.; Murali, S.; Cai, W.; Li, X.; Suk, J. W.; Pott, J. R.; Ruoff, R. S. Graphene and Graphene Oxide: Synthesis, Properties, and Applications. *Adv. Mater.* **2010**, *22*, 3906–3924.

3. Huang, X.; Yin, Z.; Wu, S.; Qi, X.; He, Q.; Zhang, Q.; Yan, Q.; Boey, F.; Zhang, H. Graphene-Based Materials: Synthesis, Characterization, Properties and Applications. *Small* **2011**, *7*, 1876–1902.

4. Chung, C.; Kim, Y. K.; Shin, D.; Ryoo, S. R.; Hong, B. H.; Min, D. H. Biomedical Applications of Graphene and Graphene Oxide. *Accounts Chem. Res.* **2013**, *46*, 2211–2224.

5. Wang, Y.; Li, Z.; Wang, J.; Li, J.; Lin, Y. Graphene and Graphene Oxide: Biofunctionalization and Applications in Biotechnology. *Trands Biotechnol.* **2011**, *20*, 249–256.

6. Machado, B. F.; Serp, P. Graphene-Based Materials for Catalysis. *Catal. Sci. Technol.* **2012**, *2*, 54–75.

7. Georgakilas, V.; Tiwari, J. N.; Kemp, K. C.; Perman, J. A.; Bourlinos, A. B.; Kim, K. S.; Zboril, R. Noncovalent Functionalization of Graphene and Graphene Oxide for Energy Materials, Biosensing, Catalytic, and Biomedical Applications. *Chem. Rev.* **2016**, *116*, 5464−5519.

8. An, D.; Yang, L.; Wang, T. J.; Liu, B. Separation Performance of Graphene Oxide Membrane in Aqueous Solution. *Ind. Eng. Chem. Res.* **2016**, *55*, 4803−4810.

9. Staudenmaier, L. Verfahren zur Darstellung der Graphitsäure. *Ber. Dtsch. Chem. Ges.* **1898**, *31*, 1481–1487.

10. Brodie, B. C. On the Atomic Weight of Graphite. *Trans. R. Soc. London* **1859**, *149*, 249–259.

11. Peng, L.; Xu, Z.; Liu, Z.; Wei, Y.; Sun, H.; Li, Z.; Zhao, X.; Gao, C. An Iron-Based Green Approach to 1-h Production of Single-Layer Graphene Oxide. *Nat. Commun.* **2015**, *6*, 5716.

12. Sofer Z.; Luxa, J.; Jankovský, O.; Sedmidubský D.; Bystroň, T; Pumera, M. Synthesis of Graphene Oxide by Oxidation of Graphite with Ferrate (VI) Compounds: Myth or Reality? *Angew. Chem. Int. Ed.* **2016**, *55*, 11965–11969.

13. Hummers, W. S.; Offeman, R. E. Preparation of Graphitic Oxide. *J. Am. Chem. Soc.* **1958**, *80*, 1339.

14. Kovtyukhova, N. I.; Olllivier, P. J.; Martin, B. R.; Mallouk, T. E.; Chizhik, S. A.; Buzaneva, E. V.; Gorchinskiy, A. D. Layer-by-Layer Assembly of Ultrathin Composite Films from Micron-sized Graphite Oxide Sheets and Polycations. *Chem. Mater.* **1999**, *11*, 771–778.

15. Sun, J.; Yang, N.; Sun, Z.; Zeng, M.; Fu, L.; Hu, C.; Hu, S. Fully Converting Graphite into Graphene Oxide Hydrogels by Preoxidation with Impure Manganese Dioxide. *ACS Appl. Mater. Interfaces.* **2015**, *7*, 21356−21363.

16. Luo Z.; Lu, Y.; Somers, A. L.; Johnson A. T. C., High Yield Preparation of Macroscopic Graphene Oxide Membranes. *J. Am. Chem. Soc.* **2009**, *131*, 898–899.

17. Marcano, D. C.; Kosynkin, D. V.; Berlin, J. M.; Sinitskii, A.; Sun, Z.; Slesarev, A.; Alemany, L. B.; Lu, W.; Tour, J. M. Improved Synthesis of Graphene Oxide. *ACS Nano* **2010**, *4*, 4806–4814.

18. Dimiev, A. M.; Tour, J. M. Mechanism of Graphene Oxide Formation. *ACS Nano* **2014**, *8*, 3060–3068.

19. Shao, G.; Lu, Y.; Wu, F.; Yang, C.; Zeng, F.; Wu, Q. Graphene Oxide: the Mechanisms of Oxidation and Exfoliation. *J. Mater. Sci.* **2012**, *47*, 4400–4409.

20. Rasuli, R.; A. Iraji zad. Density Functional Theory Prediction for Oxidation and Exfoliation of Graphite to Graphene. *Appl. Surf. Sci.* **2010**, *256*, 7596−7599.

21. Boukhvalov, D. W. DFT Modeling of the Covalent Functionalization of Graphene: from Ideal to Realistic Models. *RSC Adv.* **2013**, *3*, 7150−7159.

22. Yang, J.; Shi, G.; Tu, Y.; Fang, H. High Correlation Between Oxidation Loci on Graphene Oxide. *Angew. Chem. Int. Ed.* **2014**, *53*, 10190–10194.

23. Sun, T.; Fabris, S. Mechanisms for Oxidative Unzipping and Cutting of Graphene. *Nano Lett.* **2012**, *12*, 17−21.

24. Li, J. L.; Kudin, K. N.; MacAllister, M. J.; Prud'homme, R. K.; Aksay, I. A.; Car, R. Oxygen-Driven Unzipping of Graphitic Materials. *Phys. Rev. Lett.* **2006**, *96*, 176101.

25. Chowdhury, D. R.; Singh, C.; Paul, A. Role of Graphite Precursor and Sodium Nitrate in Graphite Oxide Synthesis. *RSC Adv.* **2014**, *4*, 15138–15145.

26. Pastor, I. R.; Fernandez, G. R.; Rizo, H. V.; Mauricio, T.; Gullon, I. M. Towards the Understanding of the Graphene Oxide Structure: How to Control the Formation of Humic- and Fulvic-Like Oxidized Debris. *Carbon* **2015**, *84*, 229–309.

27. Daioh, H.; Mizutani, Y. Identity Period of Graphite Intercalation Compound with Sulfuric Acid. *Tanso* **1985**, *123*, 177–179.

28. Sorokina, N. E.; Shornikova, O. N.; Avdeev, V. V. Stability Limits of Graphite Intercalation Compounds in the Systems Graphite–HNO_3 (H_2SO_4)–H_2O–$KMnO_4$. *Inorg. Mater.* **2007**, *43*, 822–826.

29. Chen, J.; Zhang, Y.; Zhang, M.; Yao, B.; Li, Y.; Huang, L.; Li, C.; Shi, G. Water-Enhanced Oxidation of Graphite to Graphene Oxide with Controlled Species of Oxygenated Groups. *Chem. Sci.* **2016**, *7*, 1874–1881.

30. Sugiyama, T.; Iijima, T.; Sato, M.; Fujimoto, K. Stabilities of Metal-Halide Intercalated Graphite. *Synth. Metals* **1981**, *23*, 449–454.

31. Pan, S.; Aksay, I. A., Factors Controlling the Size of Graphene Oxide Sheets Produced via the Graphite Oxide Route. *ACS Nano* **2011**, *5*, 4073–4083.

32. Storm, M. M.; Johnsen, R. E.; Norby, P. In Situ X-ray Powder Diffraction Studies of the Synthesis of Graphene Oxide and Formation of Reduced Graphene Oxide. *J. Solid. State. Chem.* **2016**, *240*, 49–54.

33. D. J. Royer, Evidence for the Existence of the Permanganyl Ion in Sulphuric Acid Solutions of Potassium Permanganate, *J. Inorg. Nucl. Chem.* **1961**, *17*, 159–167.

34. Kang, J. H.; Kim, T.; Choi, J.; Park, J.; Kim, Y. S.; Chang, M. S.; Jung, H.; Park, K. T.; Yang, S. J.; Park, C. R., Hidden Second Oxidation Step of Hummers Method. *Chem. Mater.* **2016**, *28*, 756−764.

35. Yang, L.; Zhang, R.; Liu, B.; Wang, J.; Wang, S.; Han, M. Y.; Zhang, Z. π-Conjugated Carbon Radicals at Graphene Oxide to Initiate Ultrastrong Chemiluminescence. *Angew. Chem. Int. Ed.* **2014**, *53*, 10109−10113.

36. Morimoto, N.; Kubo, T.; Nishina, Y. Tailoring the Oxygen Content of Graphite and Reduced Graphene Oxide for Specific Applications. *Sci. Rep.* **2016**, *6*, 21715.

37. Dimiev, A.; Kosynkin, D. V.; Alemany, L. B.; Chaguine, P.; Tour, J. M. Pristine Graphite Oxide. *J. Am. Chem. Soc.* **2012**, *134*, 2815−2822.

38. Eigler, S.; Grimm, S.; Hof, F.; Hirsch, A. Graphene Oxide: A Stable Carbon Framework for Functionalization. *J. Mater. Chem. A* **2013**, *1*, 11559–11562.

39. Hofmann, U.; Frenzel, A.; Csalan, E. Die Konstitution der Graphitsaure und ihre Reaktionen, *Justus Liebigs Ann. Chem.* **1934**, *510*, 1–41.

40. Pendolino, F.; Armata, N.; Masullo, T.; Cuttitta, A. Temperature Influence on the Synthesis of Pristine Graphene Oxide and Graphite Oxide. *Mater. Chem. Phys.* **2015**, *164*, 71–77.

41. Eigler, S.; Heim, M. E.; Grimm, S.; Hofmann, P.; Kroener, W.; Geworski, A.; Dotzer, C.; Röckert, M.; Xiao, J.; Papp, C.; Lytken, O.; Steinrück, H. P.; Müller, P.; Hirsch, A. Wet Chemical Synthesis of Graphene. *Adv. Mater.* **2013**, *25*, 3583–3587.

42. Haight G. P. Jr.; Phillipson D. Hazard in "Permanganate Volcano" Demonstration. *J. Chem. Educ.* **1980**, *57*, 325.